20

# Memory Effects in Mixtures of Liquid Crystals and Anisotropic Nanoparticles

Marjan Krašna[1], Matej Cvetko[1,2], Milan Ambrožič[1] and Samo Kralj[1,3]
[1]*University of Maribor, Faculty of Natural Science and Mathematics*
[2]*Regional Development Agency Mura Ltd*
[3]*Jožef Stefan Institute, Condensed Matter Physics Department*
*Slovenia*

## 1. Introduction

For years there is a substantial interest on impact of disorder on condensed matter structural properties (Imry & Ma, 1975) (Bellini, Buscaglia, & Chiccoli, 2000) (Cleaver, Kralj, Sluckin, & Allen, 1996). Pioneering studies have been carried out in magnetic materials (Imry & Ma, 1975). In such system it has been shown that even relatively weak random perturbations could give rise to substantial degree of disorder. The main reason behind this extreme susceptibility is the existence of the Goldstone mode in the continuum field describing the orienational ordering of the system. This fluctuation mode appears unavoidably due to continuous symmetry breaking nature of the phase transition via which a lower symmetry magnetic phase was reached. For example, the Imry Ma theorem (Imry & Ma, 1975), one of the pillars of the statistical mechanics of disorder, claims, that even arbitrary weak random field type disorder could destroy long range ordering of the unperturbed phase and replace it with a short range order (SRO). Note that this theorem is still disputable because some studies claim that instead of SRO a quasi long order could be established (Cleaver, Kralj, Sluckin, & Allen, 1996).

During last decades several studies on disorder have been carried out in different liquid crystal phases (LC) (Oxford University, 1996), which are typical soft matter representatives. These phases owe their softness to continuous symmetry breaking phase transitions via which these phases are reached on lowering the symmetry. In these systems disorder has been typically introduced either by confining soft materials to various porous matrices (e.g., aerogels (Bellini, Clark, & Muzny, 1992), Russian glasses (Aliev & Breganov, 1989), Vycor glass (Jin & Finotello, 2001), Control Pore Glasses (Kralj, et al., 2007) or by mixing them with different particles (Bellini, Radzihovsky, Toner, & Clark, 2001) (Hourri, Bose, & Thoen, 2001) of nm (nanoparticles) or micrometer (colloids) dimensions. It has been shown that the impact of disorder could be dominant in some measured quantities. In particular the validity of Imry-Ma theorem in LC-aerosil mixtures was proven (Bellini, Buscaglia, & Chiccoli, 2000).

In our contribution we show that binary mixtures of LC and rod-like nanoparticles (NPs) could also exhibit random field-type behavior if concentration $p$ of NPs is in adequate regime. Consequently, such systems could be potentially exploited as memory devices. The plan of the contribution is as follows. In Sec. II we present the semi-microscopic model used

to study structural properties of LCs perturbed by NPs. We express the interaction potential, simulation method and measured quantities. In Sec. III the results of our simulations are presented. We calculate percolation characteristics of systems of our interest. Then we first study examples where LC is perturbed by quenched random field-type interactions. We analyze behavior i) in the absence of an external ordering field $B$, ii) in presence of $B$, and iii) $B$ induced memory effects. Afterwards we demonstrate conditions for which LC-NP mixtures effectively behave like a random field-type system.

## 2. Model

### 2.1 Interaction potential

We consider a bicomponent mixture of liquid crystals (LCs) and anisotropic nanoparticles (NPs). A lattice-spin type model (Lebwohl & Lasher, 1972) (Romano, 2002) (Bradač, Kralj, Svetec, & Zumer, 2003) is used where the lattice points form a three dimensional cubic lattice with the lattice constant $a_0$. The number of sites equals $N^3$, where we typically set $N = 80$. The NPs are randomly distributed within the lattice with probability $p$ (For $p = 1$ all the sites are occupied by NPs).

Local orientation of a LC molecule or a nanoparticle at a site $\vec{r}_i$ is given by unit vectors $\vec{s}_i$ and $\vec{m}_i$, respectively. We henceforth refer to these quantities as nematic and NP spins. We take into account the head-to-tail invariance of LC molecules (De Gennes & Prost, 1993), i.e., the states $\pm\vec{s}_i$ are equivalent. It is tempting to identify the quantity $\vec{s}_i$ with the local nematic director which appears in continuum theories. We allow NPs to be ferromagnetic or ferroelectric. In these cases $\vec{m}_i$ points along the corresponding dipole orientation. Also other sources of NP anisotropy are encompassed within the model. For example, $\vec{m}_i$ might simulate a local topological dipole consisting of pair defect-antidefect.

The interaction energy $W$ of the system is given by (Lebwohl & Lasher, 1972) (Romano, 2002) (Bradač, Kralj, Svetec, & Zumer, 2003)

$$W = -\sum_{ij} J_{ij}^{(LC)}(\vec{s}_i \cdot \vec{s}_j)^2 - \sum_{ij} J_{ij}^{(NP)}\vec{m}_i \cdot \vec{m}_j - \sum_{ij} w_{ij}(\vec{s}_i \cdot \vec{m}_j)^2 - \sum_i \chi_B B^2(\vec{s}_i \cdot \vec{e}_B)^2 - \sum_i B\vec{m}_i \cdot \vec{e}_B \qquad (1)$$

The constants $J_{ij}^{(LC)}$, $J_{ij}^{(NP)}$, and $w_{ij}$ describe pairwise coupling strengths LC-LC, NP-NP, and LC-NP, respectively. The last two terms take into account a presence of *homogeneous* external electric or magnetic field $\vec{B} = B\vec{e}_B$, where $\vec{e}_B$ is a unit vector; the $B^2$ term acts on nematic spins while linear $B$ term acts on magnetic spins.

Only first neighbor interactions are considered. Therefore $J_{ij}^{(LC)}$, $J_{ij}^{(NP)}$, and $w_{ij}$ are different from zero only if $i$ and $j$ denote neighbouring molecules. The Lebwohl Lasher-type term describes interaction among LC molecules, where $J_{ij}^{(LC)} = J > 0$. Therefore, a pair of LC molecules tend to orient either parallel or antiparallel. The coupling between neighboring NPs is determined with $J_{ij}^{(NP)} = J_{NP} > 0$ which enforces parallel orientation. On the contrary, neighboring LC-NP pairs tend to be aligned perpendicularly by the interaction strength $w_{ij} = w < 0$.

We also consider the case when the anisotropic particles act as a *random* field. For this purpose we use the interaction potential (Bellini, Buscaglia, & Chiccoli, 2000) (Romano, 2002).

$$W^{(RAN)} = -\sum_{ij} J_{ij}^{(LC)} (\vec{s}_i \cdot \vec{s}_j)^2 - \sum_i w_i (\vec{s}_i \cdot \vec{e}_i)^2 - \sum_i B^2 (\vec{s}_i \cdot \vec{e}_B)^2 \tag{2}$$

The first LC-LC ordering term is already described above. In the second term the quantity $w_i$ plays the role of a local quenched field. LC molecules are occupying all the lattice sites and only a fraction $p$ of them experiences the quenched random field. These "occupied" sites are chosen randomly. In the cases $w_i = w > 0$ or $w < 0$ the random field tends to align LC molecules along $\vec{e}_i$ or perpendicular to it, respectively. The direction of the unit vector $\vec{e}_i$ is chosen randomly and is distributed uniformly on the surface of a sphere.
In all subsequent work, distances are scaled with respect to $a_0$ and interaction energies are measured with respect to $J$ (i.e., $J = 1$).

### 2.2 Simulation method

Each site is enumerated with three indices: $p$, $q$, $r$, where $1 \le p \le N$, $1 \le q \le N$, $1 \le r \le N$. The equilibrium director configuration is obtained by minimizing the total interaction energy with respect to all the directors by taking into account the normalization condition $\left|\vec{n}_{pqr}\right|^2 = 1$. The resulting potential to be mimimized reads $W^* = \sum_{pqr} W_{pqr}{}^*$, where

$$W_{pqr}{}^* = \lambda_{pqr}\left(\left|\vec{n}_{pqr}\right|^2 - 1\right) + W_{pqr}, \tag{3}$$

and $\lambda_{pqr}$ are Lagrange multipliers. We minimize the potential $W^*$ and obtain the following set of $N^3$ equations which are solved numerically. We give here the corresponding equations just for the free energy given in Eq. (2).

$$\sum_{p'q'r'} \vec{g}(\vec{n}_{pqr}, \vec{n}_{p'q'r'}) + w_{pqr}\vec{g}(\vec{n}_{pqr}, \vec{e}_{pqr}) + B^2\vec{g}(\vec{n}_{pqr}, \vec{e}_B) = 0, \tag{4}$$

where the vector function $\vec{g}$ is defined as

$$\vec{g}(\vec{v}_1, \vec{v}_2) = (\vec{v}_1 \cdot \vec{v}_2)\left[\vec{v}_2 - (\vec{v}_1 \cdot \vec{v}_2)\vec{v}_1\right]. \tag{5}$$

The system of Eq. (4) is solved by relaxation method which has been proved fast and reliable. We used periodic boundary conditions for spins at the cell boundaries, for instance, the "right" neighbor of the spin with indices ($N$, $q$, $r$) is the spin with indices (1, $q$, $r$), and similarly in other boundaries.

### 2.3 Calculated parameters

In simulations we either originate from randomly distributed orientations of directors, or from homogeneously aligned samples along a symmetry breaking direction. In the latter case the directors are initially homogeneously aligned along $\vec{e}_x$. We henceforth refer to these cases as the i) *random* and ii) *homogeneous* case, respectively. The i) *random* case can be experimentally realized by quenching the system from the isotropic phase to the ordered phase without an external field (i.e., $B = 0$). This can be achieved either via a sudden

decrease of temperature or sudden increase of pressure. ii) The *homogeneous* case can be realized by applying first a strong homogeneous external field $\vec{B}$ along a symmetry breaking direction. After a complete alignment is achieved the field is switched off.
In order to diminish the influence of statistical variations we carry out several simulations (typically $N_{\mathrm{rep}} \sim 10$) for a given set of parameters (i.e., $w$, $p$ and $a$ chosen initial condition).
From obtained configurations of directors we calculate the orientational correlation function $G(r)$. It measures orientational correlation of directors as a function of their mutual separation $r$. We define it as (Cvetko, Ambrozic, & Kralj, 2009)

$$G(r) = \frac{1}{2}\left\langle 3\left(\vec{s}_i \cdot \vec{s}_j\right)^2 - 1 \right\rangle \tag{6}$$

The brackets $\langle ... \rangle$ denote the average over all lattice sites that are separated for a distance $r$. If the directors are completely correlated (i.e. homogeneously aligned along a symmetry breaking direction) it follows $G(r) = 1$. On the other hand $G(r) = 0$ reflects completely uncorrelated directors. Since each director is parallel with itself, it holds $G(0) = 1$. The correlation function is a decreasing function of the distance $r$. We performed several tests to verify the isotropic character of $G(r)$ , i.e. $G(\vec{r}) = G(r)$ .
In order to obtain structural details from a calculated $G(r)$ dependence we fit it with the ansatz (Cvetko, Ambrozic, & Kralj, 2009)

$$G(r) = (1 - s)e^{-(r/\xi)^m} + s \tag{7}$$

where the $\xi$, $m$, and $s$ are adjustable parameters. In simulations distances are scaled with respect to $a_0$ (the nearest neighbour distance). The quantity $\xi$ estimates the average domain length (the coherence length) of the system. Over this length the nematic spins are relatively well correlated. The distribution width of $\xi$ values is measured by $m$. Dominance of a single coherence length in the system is signalled by $m = 1$. A magnitude and system size dependence of $s$ reveals the degree of ordering within the system. The case $s = 0$ indicates the short range order (SRO). A finite value of $s$ reveals either the long range order (LRO) or quasi long range order (QLRO). To distinguish between these two cases a finite size analysis $s(N)$ must be carried out. If $s(N)$ saturates at a finite value the system exhibits LRO. If $s(N)$ dependence exhibits algebraic dependence on $N$ the system possesses QLRO (Cvetko, Ambrozic, & Kralj, 2009).
Note that the external ordering field ($B$) and NPs could introduce additional characteristic scales into the system. The relative strength of elastic and external ordering field contribution is measured by the external field extrapolation length (De Gennes & Prost, 1993) $\xi_B \sim \sqrt{J}/B$ . In the case of ordered LC-substrate interfaces the relative importance of surface anchoring term is measured by the surface extrapolation length (De Gennes & Prost, 1993) $d_e \sim J/w$ . The external ordering field is expected to override the surface anchoring tendency in the limit $d_e/\xi_B >> 1$ . However, if LC-substrate interfaces introduce a disorder into the system, then instead of $d_e$ the so called Imry-Ma scale $\xi_{IM}$ characterizes the ordering of the system. It expresses the relative importance of the elastic ordering and local surface term. It roughly holds (Imri & Ma, 1975):

$$\xi_{IM} \propto w_{dis}^{\frac{2}{d-4}} \tag{8}$$

where $w_{dis} \propto w$ measures the disorder strength. Parameter $d$ in the exponent of Eq. (8) denotes the dimensionality of physical system: in our case $d = 3$, thus $\xi_{IM} \propto w_{dis}^{-2}$.

## 3. Results

### 3.1 Percolation

One expects that systems might show qualitatively different behaviour above and below the percolation threshold $p = p_c$ of *impurities*. For this reason we first analyze the percolation behaviour of 3*D* systems for typical cell dimensions implemented in our simulations.

On increasing the concentration $p$ of *impurities* a percolation threshold is reached at $p = p_c$. This is well manifested in the $P(p)$ dependence shown in Fig. 1, where $P$ stands for the probability that there exists a connected path of *impurity* sites between the bottom and upper (or left and right) side of the simulation cell. In the thermodynamic limit $N \to \infty$ the $P(p)$ dependence displays a phase transition type of behaviour, where $P$ plays the role of order parameter, i.e., $P(p > p_c) = 1$ and $P(p < p_c) = 0$. For a finite simulation cell a pretransitional tail appears below $p_c$, and at $p \sim 0.30$ the $P(p)$ steepness decreases with decreasing $N$. In simulations we use large enough values of $N$, so that finite size effects are negligible.

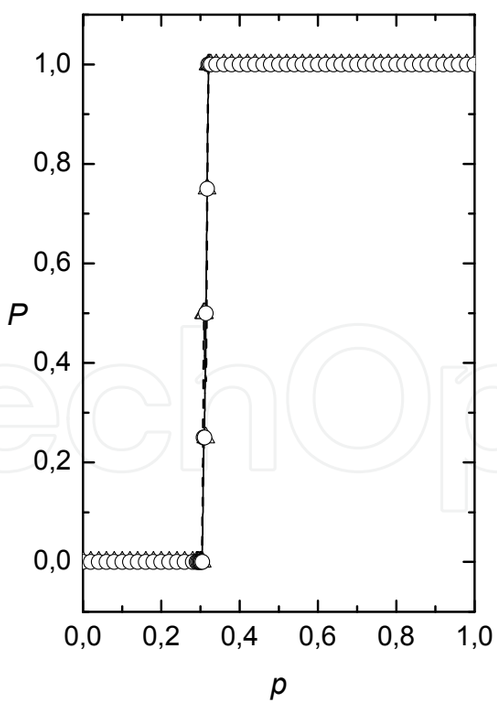


Fig. 1. The percolation probability $P$ as a function of $p$ and system size $N^3$. For a finite value of $N$ the percolation threshold ($p = p_c$) is defined as the point where $P = 0.5$. We obtain $p_c \sim 0.3$ roughly irrespective of the system size. (Δ) $N = 60$; (○) $N = 80$.

### 3.2 Structural properties in absence of external fields

We first consider the case where LC is perturbed by random field. Therefore LC configurations are solved by minimizing potential given by Eq. (2).

In Fig. 2 we plot typical correlation functions for the *random* and *homogeneous* initial conditions. One sees that in the *random* case correlations vanish for $r \gg \xi$ (i.e., $s = 0$) which is characteristic for SRO. On the contrary $G(r)$ dependencies obtained from *homogeneous* initial condition yield $s > 0$.

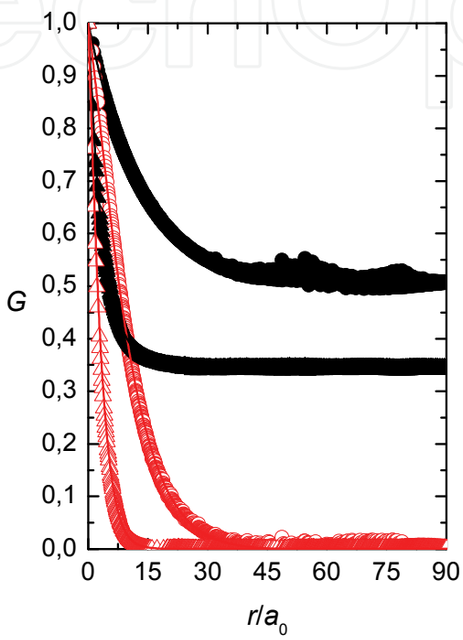


Fig. 2. $G(r)$ for $p > p_c$ and $p < p_c$ for the *homogeneous* and *random* case, $B = 0$, $w = 3$, $p_c \sim 0.3$, $N = 80$. (•) $p = 0.2$, *homogeneous*; (▲) $p = 0.7$, *homogeneous*; (○) $p = 0.2$, *random*; (Δ) $p = 0.7$, *random*.

More structural details as $p$ is varied for a relatively weak anchoring ($w = 3$) are given in Fig. 3. By fitting simulation results with Eq. (7) we obtained $\xi(p)$, $m(p)$ and $s(p)$ dependences that are shown in Fig. 3. One of the key results is that values of $\xi$ strongly depend on the history of systems for a weak enough anchoring strength $w$. A typical domain size is larger if one originates from the *homogeneous* initial configuration. We obtained a scaling relation between $\xi$ and $p$, which is again history dependent. We obtain $\xi \propto p^{-0.92\pm0.03}$ for the *homogeneous* case and $\xi \propto p^{-0.95\pm0.02}$ for the *random* case.

Information on distribution of domain coherence lengths about their mean value $\xi$ is given in Fig. 3b where we plot $m(p)$. For the *homogeneous* case we obtain $m \sim 0.95$, and for the *random* case $m \sim 1.17$. A larger value of $m$ for the *random* case signals broader distribution of domain coherence length values in comparison with the *homogeneous* case. Our simulations do not reveal any systematic changes in $m$ as $p$ is varied. Note that values of $m$ are strongly scattered because structural details of $G(r)$ are relatively weakly $m$-dependent.

In Fig. 3c we plot $s(p)$. In the *random* case we obtain $s = 0$ for any $p$. Therefore, if one starts from isotropically distributed orientations of $\vec{s}_i$, then final configurations exhibit SRO. In

the *homogeneous* case $s$ gradually decreases with $p$, but remains finite for the chosen anchoring strength ($w$ = 3).

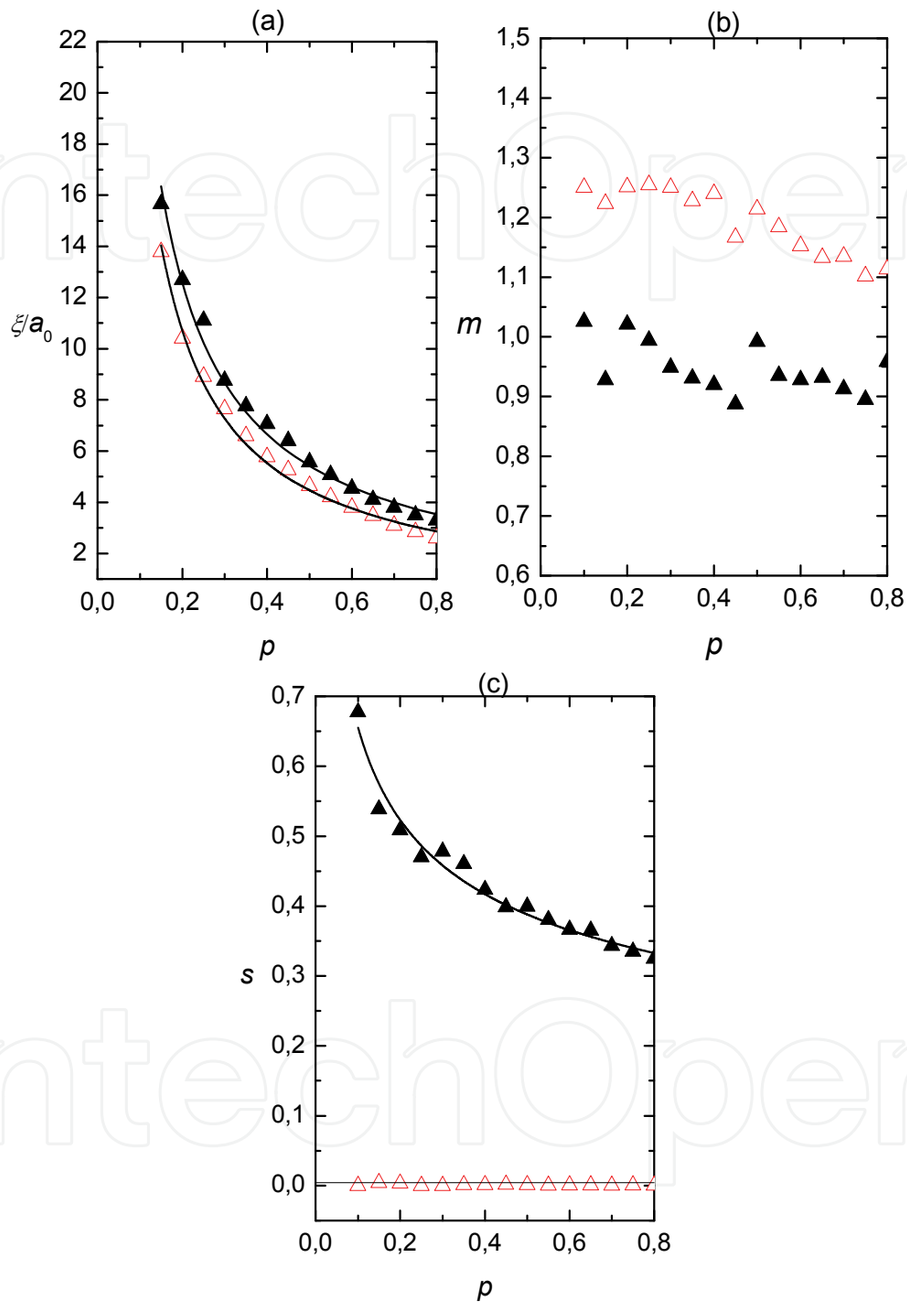


Fig. 3. Structural characteristics as $p$ is varied for $B$ = 0 and $w$ = 3. a) $\xi(p)$, b) $m(p)$, c) $s(p)$. (▲) *homogeneous*, (Δ) *random*. Lines denote the fits to power law.

For two concentrations we carried out finite size analysis, which is shown in Fig. 4. One sees that $s(N)$ dependencies saturate at a finite value of $s$, which is a signature of long-range order. We carry out simulations up to values $N$ = 140.

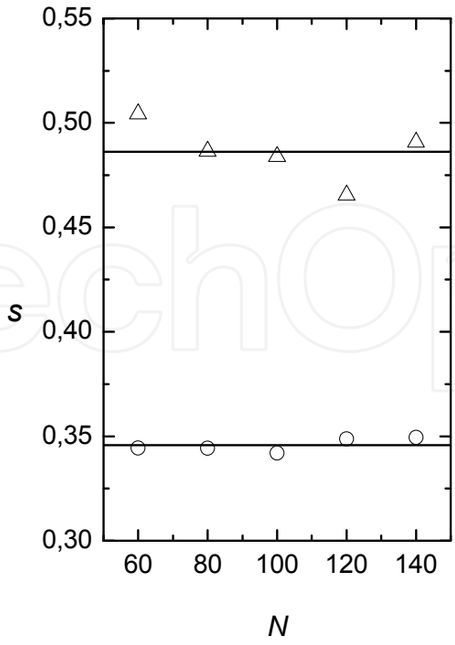


Fig. 4. Finite size analysis $s(N)$ for $p < p_c$ and $p > p_c$ for the *homogeneous* case; $B = 0$, $w = 3$, (Δ) $p = 0.2$; (○) $p = 0.7$. Lines denote average values of $s$.

We now examine the $\xi(w)$ dependence. The Imry-Ma (Imry & Ma, 1975) theorem makes a specific prediction that this obeys the universal scaling law in Eq. (8): $\xi \propto w^{-2}$ holds for $d = 3$. We have analyzed results for $p = 0.3$, $p = 0.5$, and $p = 0.7$, using both random and homogeneous initial configurations and we fitted results with

$$\xi = \xi_0 w^{-\gamma} + \xi_\infty \tag{9}$$

We expect that even in the strong anchoring limit, the finite size of the simulation cells will induce a non-zero coherence length. The fit with Eq. (9) shows Imry-Ma behavior at low $w$ only for cases where we originate from *random* initial configurations. The fitting parameters for some calculations are summarized in Table 1.

| Initial condition | p | γ | $\xi_0$ | $\xi_\infty$ |
|---|---|---|---|---|
| r (*random*) | 0.3 | 2.11±0.33 | 62±17 | 1.38±0.57 |
| r (*random*) | 0.5 | 1.97±0.19 | 37±4 | 0.35±0.32 |
| r (*random*) | 0.7 | 2.20±0.32 | 36±7 | 0.00±0.36 |
| h (*homogeneus*) | 0.3 | 3.29±0.23 | 297±60 | 0.90±0.28 |
| h (*homogeneus*) | 0.5 | 3.29±0.13 | 159±14 | 0.80±0.15 |
| h (homogeneus) | 0.7 | 3.15±0.26 | 99±18 | 0.50±0.22 |

Table 1. Values of fitting parameters defined by Eq. (9) for representative simulation runs.

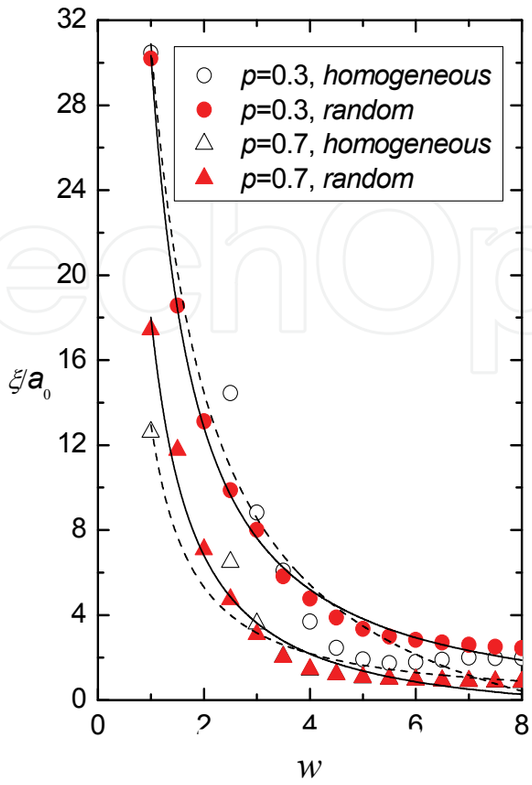


Fig. 5. $\xi(w)$ variations for different initial configurations for $N = 80$. Imry-Ma theorem is obeyed only for the *random* initial configuration.

### 3.3 External field effect

We next include external field $B$ and still consider system described by interactional potential given by Eq. (2). A typical $G(r)$dependence is shown in Fig. 6 where we see the impact of $B$. We plot $G(r)$ for both *homogeneous* and *random* initial configuration in the presence of external field and without it. For $B = 0$ it holds $\xi^{(\mathrm{hom})} > \xi^{(\mathrm{ran})}$ , where superscripts (hom) and (ran) denote correlation lengths in samples with *homogeneous* and *random initial* configurations, respectively. The reasons behind this are stronger elastic frustrations in the latter case (denotation *random samples*). Furthermore, $\xi^{(\mathrm{ran})}$ roughly obeys the Imry-Ma scaling for low enough external fields (i.e. $\xi^{(\mathrm{ran})} < < \xi_B$ where $\xi_B \sim \sqrt{J/B}$ ), suggesting $\xi^{(\mathrm{ran})} \sim \xi_{IM}$. The presence of $B$ becomes apparent when $\xi_B < \xi_{IM}$, which is shown in Fig. 6.
In Fig. 6 we see that the presence of external field can enforce a finite value of $s$ also in *random samples*.
In Fig. 7 we plot $\xi$ as a function of $1/B$ for both *homogeneous* and *random samples*. For strong enough magnetic fields one expects $\xi \sim \xi_B \propto 1/B$. On the other hand for a weak enough $B$ the value of $\xi$ is dominantly influenced by the disorder strength. Indeed, we observe a crossover behavior in $\xi(B)$ dependence on varying $B$. The crossover between two qualitatively different regimes roughly takes place at the crossover field $B_c$. We define it as the field below which the difference between $\xi^{(\mathrm{ran})}$ and $\xi^{(\mathrm{hom})}$ is apparent. Below $B_c$ the

*disordered regime* takes place, where $\xi$ exhibits weak dependence on $B$, i.e. $\xi \sim \xi_{IM}$. Above $B_c$ the *ordered regime* exists, where $\xi \sim \xi_B \propto 1/B$. Therefore, for $B > B_c$ it holds $\xi^{(\mathrm{ran})} \sim \xi^{(\mathrm{hom})} \sim \xi_B$ and in the *random regime* one observes $\xi^{(\mathrm{hom})} > \xi^{(\mathrm{ran})} \sim \xi_{IM}$.

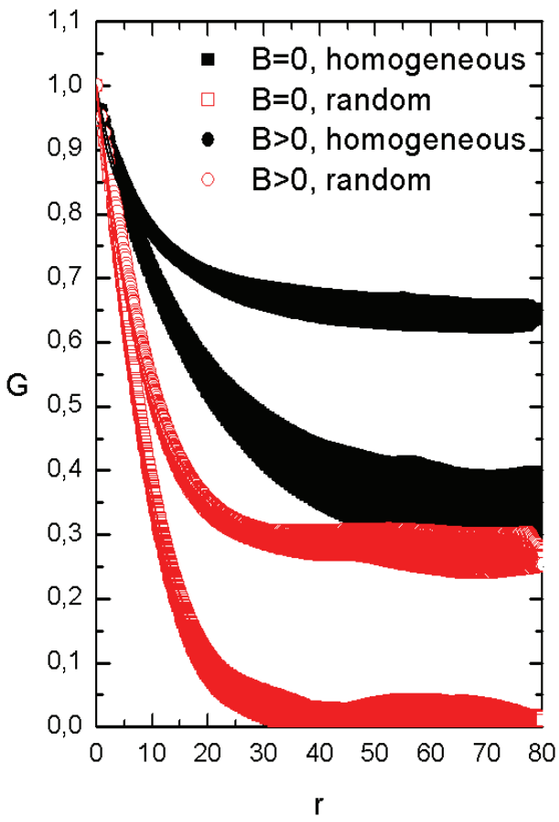


Fig. 6. The orientational correlation function as a function of separation $r$ between LC molecules. In *random samples* $G(r)$ vanishes for large enough values of $r$ for $B = 0$ while in *homogeneus samples* it could saturate at a finite plateau (if $p$ or $w$ are low enough). For $B > 0$ a finite plateau can be observed also in *random samples*. Parameters: $p = 0.3$, $w = 2.5$.

The corresponding $s(B)$ dependence is shown in Fig. 8. As expected $s$ monotonously increases on increasing $B$, because the external field tends to increase the degree of ordering. Note that in *random samples* $s(B = 0) = 0$ and the presence of $B$ gives rise to $s > 0$.

In Fig. 9 we show $m(B)$ dependence. For weak enough fields ($B << B_c$) one typically observes $m^{(\mathrm{ran})} > m^{(\mathrm{hom})} \approx 1$. Therefore, in *random samples* we have larger dispersion of $\xi$ values than in *homogeneous samples*. With the increasing external field both $m^{(\mathrm{ran})}$ and $m^{(\mathrm{hom})}$ asymptotically approach the value $m = 1$. In the latter case the distribution of $\xi$ vales is sharply centered at $\xi \sim \xi_B$.

The crossover field $B_c$ as a function of $p$ is shown in Fig. 10. Indicated lines roughly separate ergodic ($B > B_c$) and nonergodic regimes ($B < B_c$). With increasing $p$ one the degree of frustration within the system increases. Consequently larger values of $B$ are needed to erase disorders induced memory effects.

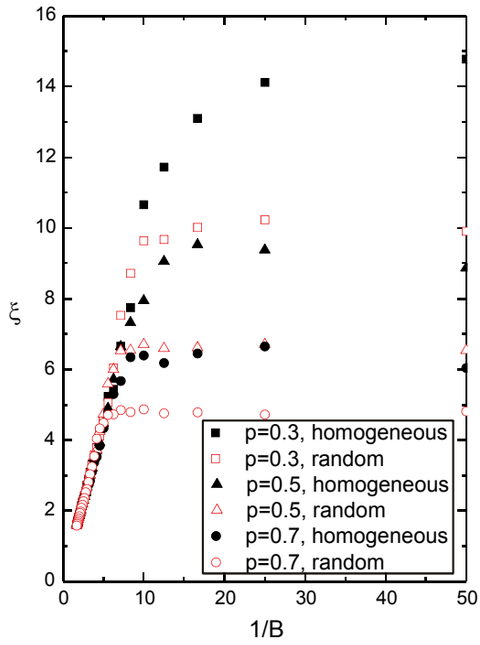


Fig. 7. Correlation length $\xi$ as a function of $1/B$ for *homogeneous* and *random samples* for three different concentrations of impurities. The $\xi(B)$ dependence displays a crossover between the *disordered* and *ordered regime*. The *disordered regimes* extends at ($B > B_c$), where $\xi^{(\mathrm{hom})} > \xi^{(\mathrm{ran})}$. In the *ordered regime* ($B < B_c$) one observes $\xi^{(\mathrm{ran})} \sim \xi^{(\mathrm{hom})} \sim \xi_B$. Parameters: $w = 2.5$, $N = 100$.

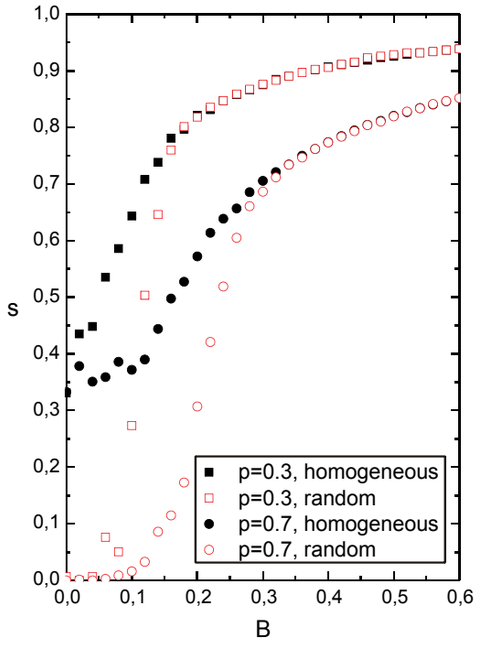


Fig. 8. The $s(B)$ dependence for *homogeneous* and *random samples* for two different $p$. For $s(B = 0)$ we obtain $s^{(\mathrm{ran})} = 0$. In the *disordered regime* it holds $s^{(\mathrm{hom})} > s^{(\mathrm{ran})}$ and $s^{(\mathrm{hom})} \sim s^{(\mathrm{ran})}$ in the *ordered regime*. Parameters: $w = 2.5$, $N = 100$.

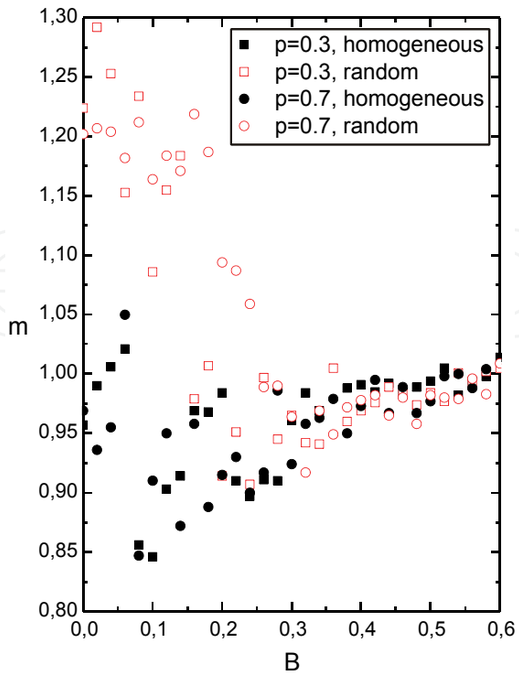


Fig. 9. The $m(B)$ dependence for *homogeneous* and *random samples* for two different $p$. In the *disordered regime* it holds $m^{(\mathrm{ran})} > m^{(\mathrm{hom})} \approx 1$. In the *ordered regime* we obtain $m^{(\mathrm{ran})} \sim m^{(\mathrm{hom})}$ which asymptotically approach one on increasing $B$. Parameters: $w = 2.5$, $N = 100$.

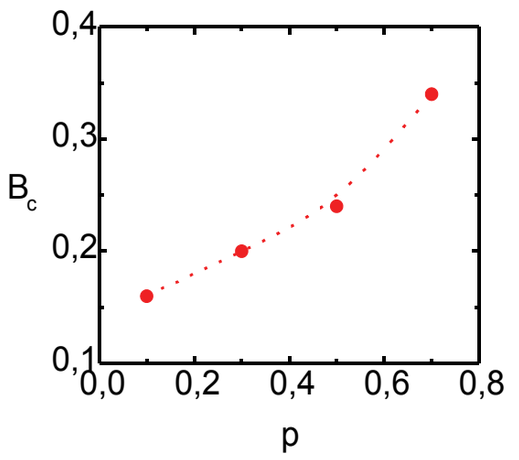


Fig. 10. The crossover field $B_c$ on varying $p$. Indicated dotted curve rougly separates ergodic ($B > B_c$) and nonergodic regimes ($B < B_c$). With increasing $p$ one the degree of frustration within the system increases. Consequently larger values of $B$ are needed to erase disorders induced memory effects. The points are calculated and the dotted line serves as a guide for the eye. Parameters: $w = 2.5$, $N = 100$.

### 3.4 Memory effects

We further analyze how one could manipulate the domain-type ordering with external magnetic or electric ordering field. For this purpose we originate from the *random* initial configuration. We then apply an external field of strength $B$ and calculate configuration for different concentrations of *impurities*. Then we switch off the field and calculate again the configuration, to which we henceforth refer as the *switch-off configuration*. The corresponding calculated $s$ and $\xi$ behaviour is shown in Fig. 11 and Fig. 12. Dashed lines mark values of observables in the presence of field of strength $B$, while full lines mark values after the field was switched off. From Fig. 11 we see that the presence of external field develops QLRO or LRO (we have not carried time consuming finite size analysis to distinguish between the two cases). This range of ordering remained as the field was switched off, although the correlation strength is reduced. Note that above the threshold field strength the degree of ordering in the *switch-off configuration* is saturated, i.e., becomes independent of $B$.

The corresponding changes in $\xi$ are shown in Fig. 12. With increasing $B$ the $\xi$ values for samples with different $p$ decrease and converge to the same value, which is equal to the external field coherence length. In the *switched-off configuration* the average domain coherence length increases and again for a large enough value of $B$ saturates at a fixed value.

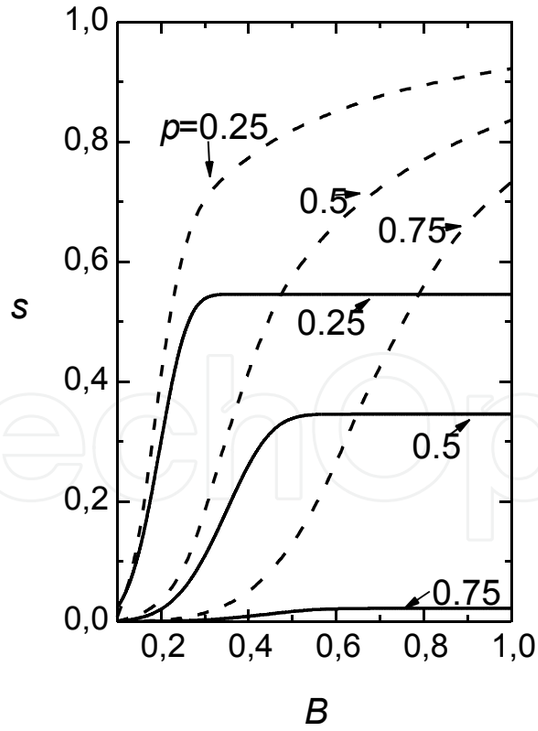


Fig. 11. $s(B)$ for $w = 4$, $N = 60$; *random* case. Dashed curves: configurations are calculated in the presence of external field $B$. Full curves: configurations are calculated after the field was switched off.

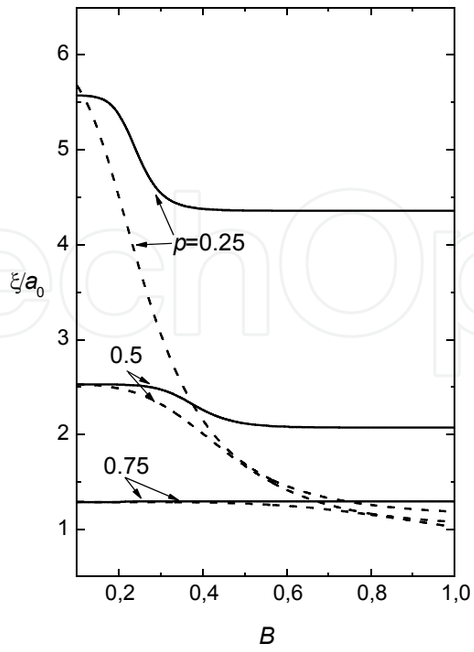


Fig. 12. $\xi(B)$ for $w = 4$, $N = 60$; *random* case. Dashed curves: configurations are calculated in the presence of external field $B$. Full curves: configurations are calculated after the field was switched off.

## 4. Mixtures

We next consider a mixture of LCs and NPs. The presence of NPs enforces to LC a certain amount of disorder. Our expectation is that if one quenches the system from the isotropic phase the established domain pattern could be stabilized by NPs. In the following we show that there indeed exists a regime where a binary mixture behaves like LC system perturbed by a random field-type perturbation.

We calculate the LC correlation by minimizing Eq. (1). In simulations mixtures are quenched from the isotropic phase. The LC correlation function is calculated from Eq. (6) from which we extract $\xi$ and $s$ by using Eq. (7). Typical results are shown in Fig. 13 where we plot $\xi(p)$ and $s(p)$. A strong presence of disorder is observed for concentrations roughly between $p = 0.1$ till percolation threshold. This is indicated by $s(p) \sim 0$, which signals presence of short range order. For $p > p_c$ the $s(p)$ becomes again apparently larger than zero.

## 5. Conclusions

We study structural properties of nematic LC phase which is perturbed by presence of anisotropic NPs. Simulations are performed at the semi-microscopic level, where orientational ordering of LCs and NPs is described by vector fields taking into account head-to-tail invariance. Such modeling approximately describes entities exhibiting cylindrical symmetry. We focused on orientational ordering of LC molecules as a function of concentration p of NPs or random sites, interaction strength w between LC molecules and perturbing agents and external ordering field strength $B$.

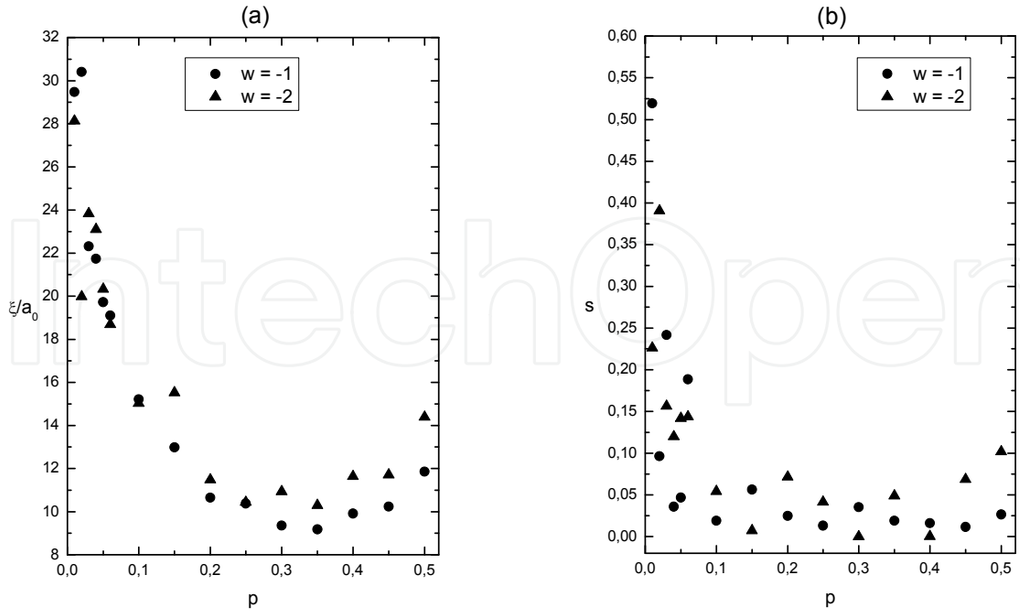


Fig. 13. Structural characteristics for the mixture. One sees that the *random* field regime extends roughly between $p = p_{RF} \sim 0.1$ and $p = p_c \sim 0.3$. a) $\xi(p)$ and b) $s(p)$ dependence. The other interaction constants are set to 1.

We determined percolation properties of NPs, which exhibit the percolation threshold $p_c \sim 0.3$ in three dimensions. Then we first studied cases, where impact of NPs could be mimicked by a random field type interaction. Studies for $B = 0$ showed that the Imry-Ma type behavior is expected only in the case, where ensembles were quenched from the isotropic phase. In this case a short range ordering is realized. Studies in presence of an external ordering field $B$ followed. We estimated boundaries separating ergodic and nonergodic regimes. We explored memory effects by exposing LCs to different strengths of $B$ and then switching it off. We determined regimes where memory effects are apparent and are roughly proportional to values of $B$. Finally we demonstrated under which conditions structural behavior in mixtures of NPs and LCs could be mimicked by random-field type models. The findings of our investigations might be useful in order to design soft matter based memory devices in mixtures of LCs and appropriate NPs.

## 6. Acknowledgments

Matej Cvetko acknowledges support of the EU European Social Fund. Operation is performed within the Operative program for development of human resources for the period 2007-2013.

## 7. References

Aliev, F. M., & Breganov, M. N. (1989). Dielectric polarization and dynamics of molecular-motion of polar liquid-crystals in micropores and macropores. *Zhurnal Eksperimentalnoi i Teoreticheskoi Fiziki, 95*(1), 122-138.

Bellini, T., Buscaglia, M., & Chiccoli, C. (2000). Nematics with quenched disorder: What is left when long range order is disrupted? *Physical Review Letters, 85*(5), 1008-1011.

Bellini, T., Clark, N. A., & Muzny, C. D. (1992). Phase-behavior of the liquid-crystal 8cb in a silica aerogel. *Physical Review Letters, 69*(5), 788-791.

Bellini, T., Radzihovsky, L., Toner, J., & Clark, N. A. (2001). Universality and scaling in the disordering of a smectic liquid crystal. *SCIENCE, 294*(5544), 1074-1079.

Bradač, Z., Kralj, S., Svetec, M., & Zumer, S. (2003). Annihilation of nematic point defects: Postcollision scenarios. *Physical Review E, 67*(5), 050702.

Cleaver, D. J., Kralj, S., Sluckin, T. J., & Allen, M. P. (1996). *Liquid Crystals in Complex Geometries: Formed by Polymer and Porous Networks.* London: Oxford University Press.

Cvetko, M., Ambrozic, M., & Kralj, S. (2009). Memory effects in randomly perturbed systems exhibiting continuous symmetry breaking. *Liquid Crystals, 36*(1), 33-41.

De Gennes, P. G., & Prost, J. (1993). *The Physics of Liquid Crystals.* Oxford: Oxford University Press.

Hourri, A., Bose, T. K., & Thoen, J. (2001). ffect of silica aerosil dispersions on the dielectric properties of a nematic liquid crystal. *Physical Review E, 63*(5), 051702.

Imry, Y., & Ma, S. (1975). Random-field instability of ordered state of continuous symmetry. *Physical Review Letters, 35*(21), 1399-1401.

Jin, T., & Finotello, D. (2001). Aerosil dispersed in a liquid crystal: Magnetic order and random silica disorder. *Physical Review Letters, 86*(5), 818-821.

Kralj, S., Cordoyiannis, G., Zidansek, A., Lahajnar, G., Amentsch, H., Zumer, S., et al. (2007). Presmectic wetting and supercritical-like phase behavior of octylcyanobiphenyl liquid crystal confined to controlled-pore glass matrices. *Journal of Chemical Physics, 127*(15), 154905.

Lebwohl, P. A., & Lasher, G. (1972). Nematic-liquid-crystal order - monte-carlo calculation. *Physical Review A, 6*(1), 426.

Oxford University. (1996). *Liquid Crystals in Complex Geometries Formed by Polymer and Porous Networks.* (S. Zumer, & G. Crawford, Eds.) London: Taylor & Francis.

Romano, S. (2002). Computer simulation study of a nematogenic lattice-gas model with fourth-rank interactions. *International Journal of Modern Physics, 16*(19), 2901-2915.

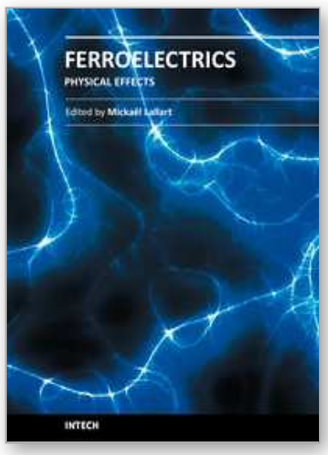


**Ferroelectrics - Physical Effects**

Edited by Dr. MickaÃ«l Lallart

ISBN 978-953-307-453-5
Hard cover, 654 pages
**Publisher** InTech
**Published online** 23, August, 2011
**Published in print edition** August, 2011

Ferroelectric materials have been and still are widely used in many applications, that have moved from sonar towards breakthrough technologies such as memories or optical devices. This book is a part of a four volume collection (covering material aspects, physical effects, characterization and modeling, and applications) and focuses on the underlying mechanisms of ferroelectric materials, including general ferroelectric effect, piezoelectricity, optical properties, and multiferroic and magnetoelectric devices. The aim of this book is to provide an up-to-date review of recent scientific findings and recent advances in the field of ferroelectric systems, allowing a deep understanding of the physical aspect of ferroelectricity.



**InTech Europe**
University Campus STeP Ri
Slavka Krautzeka 83/A
51000 Rijeka, Croatia
Phone: +385 (51) 770 447
Fax: +385 (51) 686 166
www.intechopen.com

**InTech China**
Unit 405, Office Block, Hotel Equatorial Shanghai
No.65, Yan An Road (West), Shanghai, 200040, China
中国上海市延安西路65号上海国际贵都大饭店办公楼405单元
Phone: +86-21-62489820
Fax: +86-21-62489821

IntechOpen